ABSTRACT

Name: Kurt Francis Department: Physics

Title: Evaluating Small Scintillating Cells for Digital Hadron Calorimeters

Major: Applied Physics Degree: Master of Science

Approved by: Date:

_____ _____

Dissertation Director

NORTHERN ILLINOIS UNIVERSITY

: Operated by Fermi Research Alliance, LLC under Contract No. De-AC02-07CH11359 with the United States Department of Energy.

ABSTRACT

This thesis discusses the use of scintillator cells with digital electronics as a basis for a digital hadron calorimeter. The detection of a minimum ionizing particle (MIP), analysis of crosstalk, and determination of light yield for the array of scintillating cells are described. The cells were found to have a light yield (in terms of single photoelectrons per MIP) of 7 to 13. Crosstalk due to transfer of light between adjacent cells or photomultiplier tube channels can reach 45%. Rejection versus efficiency studies show that single-channel thresholds can be set that reject noise while accepting MIP signals.

NORTHERN ILLINOIS UNIVERSITY

EVALUATING SMALL SCINTILLATING CELLS FOR DIGITAL HADRON CALORIMETERS

A THESIS SUBMITTED TO THE GRADUATE SCHOOL

IN PARTIAL FULFILLMENT OF THE REQUIREMENTS

FOR THE DEGREE

MASTER OF SCIENCE

DEPARTMENT OF PHYSICS

BY

KURT FRANCIS

DEKALB, IL

MAY 2004

Certification: In accordance with departmental and Graduate School policies, this thesis is accepted in partial fulfillment of degree requirements.

_____

Thesis Director

_____

Date

ACKNOWLEDGEMENTS

I would like to thank Sasha Dychkant, Victor Rykalin, and Manuel Martin for all of their help and assistance. I would also like to to thank Doctor Gerald Blazey, my thesis advisor, for his advice and direction and all the other members of the Northern Illinois Center for Accelerator and Detector Development.

TABLE OF CONTENTS

Page

LIST OF TABLES v

LIST OF FIGURES vi

Chapter

1. INTRODUCTION 1

2. DESCRIPTION OF A SINGLE CELL AND HARDWARE . . . 4

3. ANALYSIS OF DATA 12

3.1 Pedestal 12

3.2 MIP Curve 12

4. ANALYZING CROSSTALK 14

4.1 Demonstration of Crosstalk 14

4.2 Isolating the Cells 14

4.3 Analyzing Crosstalk at the Photomultiplier Tube 16

4.4 Summary of Crosstalk Issues 18

5. CALIBRATION AND LIGHT YIELD 22

6. CONCLUSIONS 28

REFERENCES 30

LIST OF TABLES

Table Page

1. Light Yield and ADC Count Data 27

LIST OF FIGURES

Figure		Page
1.	Structure of a single scintillating cell	4
2.	The 16 channel map of the PMT	5
3.	Diagram of the cosmic ray test stand	7
4.	Block diagram of triggering and data collection electronics . . .	8
5.	Picture of electronics hardware	8
6.	Main window of the analysis software	9
7.	Scatterplots showing the response of all cells relative to cell four .	11
8.	Example histogram	12
9.	Before and after isolation of channel four	15
10.	Crosstalk before and after isolating cells 5,6 and 8	16
11.	Abreviated scatterplot map arranged by PMT channel . . .	17
12.	Channel map of signal with only channel four connected . . .	18
13.	Efficiency and noise rejection for channel four	20
14.	Noise rejection percentage as a function of efficiency for channel four	21
15.	Shifting of single photoelectron spectrum peak relative to pedestal as filter layers are added	24

Figure Page

16. Photoelectron peak as a function of layers of filter material . . . 25

17. Number of cells versus light yield 27

CHAPTER 1

INTRODUCTION

The Tevatron proton-antiproton collider at Fermi National Accelerator Laboratory is currently the most powerful accelerator in the world available for high-energy physics (HEP) research. By the year 2007 the large hadron collider (LHC) at CERN (European Organization for Nuclear Research) will take the lead with collision energies seven times that of the Tevatron and greater luminosity [1]. Since there will still be unanswered questions about the Higgs particle and the origin of mass, supersymmetry, and the standard model of particle physics, the HEP community has already begun planning for a next-generation accelerator to complement or surpass LHC [2].

Whereas both the Tevatron and LHC accelerate protons, a favored option for the next generation involves electrons and positrons as the accelerated particles. Although the total energy would be less than the LHC, the luminosity would be higher and the interactions between electrons and positrons would be much "cleaner." Unlike hadrons, which are made out of quarks, electrons and positrons are elementary particles [3].

Both the Tevatron and LHC are synchrotrons, which contain the proton beam with a ring of magnets. Particles accelerated in this way lose energy due to synchrotron radiation. The energy loss due to synchrotron radiation is inversely proportional to the rest mass of the particle. For relatively massive particles such as protons this loss is acceptable. For less massive particles such as electrons the loss is significant. For this

reason, a positron-electron (e+/e-) collider would be a linear accelerator.

As with design of the accelerator, studies of new technology for linear accelerator detector design are also ongoing. The Northern Illinois Center for Accelerator and Detector Development (NICADD) is studying designs for a proposed linear collider accelerator detector.

Much of the interesting phenomena at a linear e+/e- collider can be detected as final-state jets of hadrons. Excellent jet energy and position resolution can be achieved by using "energy flow" or "particle flow" algorithms to combine the data from particle trackers and calorimeters[4]. In high-energy physics a calorimeter is an instrument used to measure the energy of a subatomic particle through absorption of the particle's kinetic energy in a block of matter[5]. In order to achieve the required resolution, the calorimeters must be designed with high three-dimensional resolution. An attractive approach would be the use of many small scintillating cells. To cut down on electronics costs, the electronic output of the cells could be limited to a single bit of dynamic range[6].

This thesis discusses the use of small scintillating plastic cells as a basis for digital hadron calorimeters. The light from each cell is transmitted through an optical fiber to a photomultiplier tube (PMT) channel. The PMT output is digitized with an analog to digital converter (ADC). A computer reads the data from the ADC and is used to analyze the data. For this thesis, cosmic rays were used as a “free” source of radiation. Cosmic rays reaching the laboratory are primarily muons[7]. The first phase of the project involved design, construction, and characterization of the equipment. The second phase

involved collection of cosmic ray data and analysis of crosstalk between channels. The third phase involved determination of the PMT's single photoelectron spectrum and, with that, the light yield of each cell for a single muon.

CHAPTER 2

DESCRIPTION OF A SINGLE CELL AND HARDWARE

Each cell has a regular hexagonal shape with 9.4 cm^2 area and 5 mm thickness and is made of BC408 scintillating plastic. The scintillator is a polymer with two dopants. The polymer emits light at ultraviolet wavelengths, and the dopants step the light down to blue wavelengths. As shown in Fig. 1, optical fibers are glued into a sigma-shaped groove. The glue holds the fiber in place and improves light collection by a factor of two because the glue has an index of refraction (n) closer to the plastic than air.

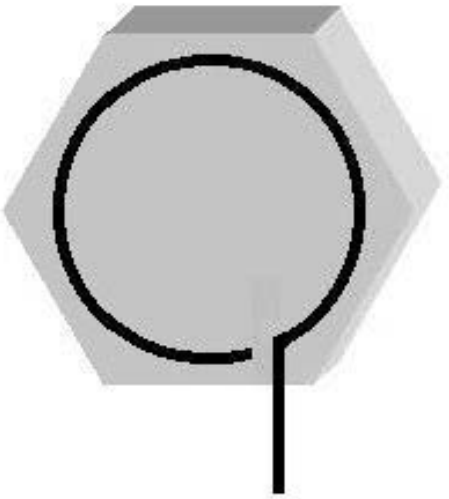

Fig. 1: Structure of a single scintillating cell.

The blue light attenuates quickly due to dispersion. To reduce light loss, the fibers are 0.94mm in outer diameter, round, blue-to-green-extended wavelength shifting (WLS)

fibers made of BCF-92 plastic. The optical fibers have n=1.8 to 1.9 with cladding of n= 1.51 to 1.52. The WLS fibers are 14cm long with approximately 8cm in the sigma groove. These fibers were then spliced to clear Kuraray double-cladded fibers approximately 165cm long to carry the optical signal to the PMT. These were then inserted into a bezel that locks ferrules into place over the PMT.

The Hamamatsu H6568 is a 16-channel PMT[8]. Fourteen of these channels were connected to hexagonal cells arranged into two layers of seven cells each. The 16-channel PMT was characterized by illuminating each channel. Inside a lightproof crate, a green LED was driven by the output of a pulse generator. The LED output was diffused and directed through an optical fiber. As shown in Fig. 2, the fibers were mapped into each of the 16 channels. The lowest reponse channel generates 63% of the signal of the strongest response channel when illuminated under the same conditions.

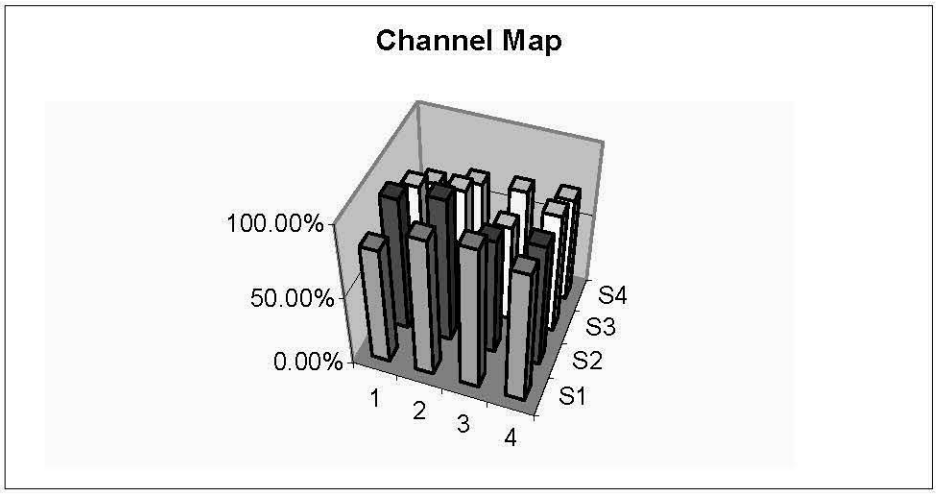

Fig. 2: The 16-channel map of the PMT. The relative response to identical input is shown.

The output of the PMT is fed through coaxial cables with a 126-nanosecond delay into a CAEN model V792 VME QDC, which will hereafter be referred to as the ADC. The V792 ADC has 32 independent channels, though only 16 were used for this experiment. The ADC is a Versa Module Europa (VME) bus protocol board mounted in a VME crate, which is connected to a computer with a VME adapter board.

As shown in Fig. 3, another set of seven cells is ganged into a FEU-115 PMT to generate a trigger signal T1. This assembly is contained in the same lightproof box as the data-collecting cells. Triggers T2 and T3 are each generated by a 14x14x0.5cm square scintillator fed into a Thorn EMI98133 RB-1102 PMT.

Each of these trigger signals is fed into a discriminator through a coaxial cable with 32ns delay. The output of each of the three discriminators is fed into a logic gate to establish a three-way coincidence. To further clean up the signal, the output of the coincidence unit is put through another discriminator before being connected to the ADC gate input. The triggering electronics are built out of NIM modules. The triggering system supplies a 50ns gate that causes the ADC to digitize all 32 channels simultaneously. See Figs. 4 and 5.

The computer runs data collection software written in the National Instruments' LabView programming environment. LabView is a graphical programming language that operates on a data-flow paradigm. LabView functions and subprograms are manipulated as icons and connected together by virtual wires[9].

The PC data collection software stores all 32 channels in one flat-text file that can easily be converted to an Excel worksheet file with each channel corresponding to one

column of the spreadsheet. Each row of the spreadsheet represents one event.

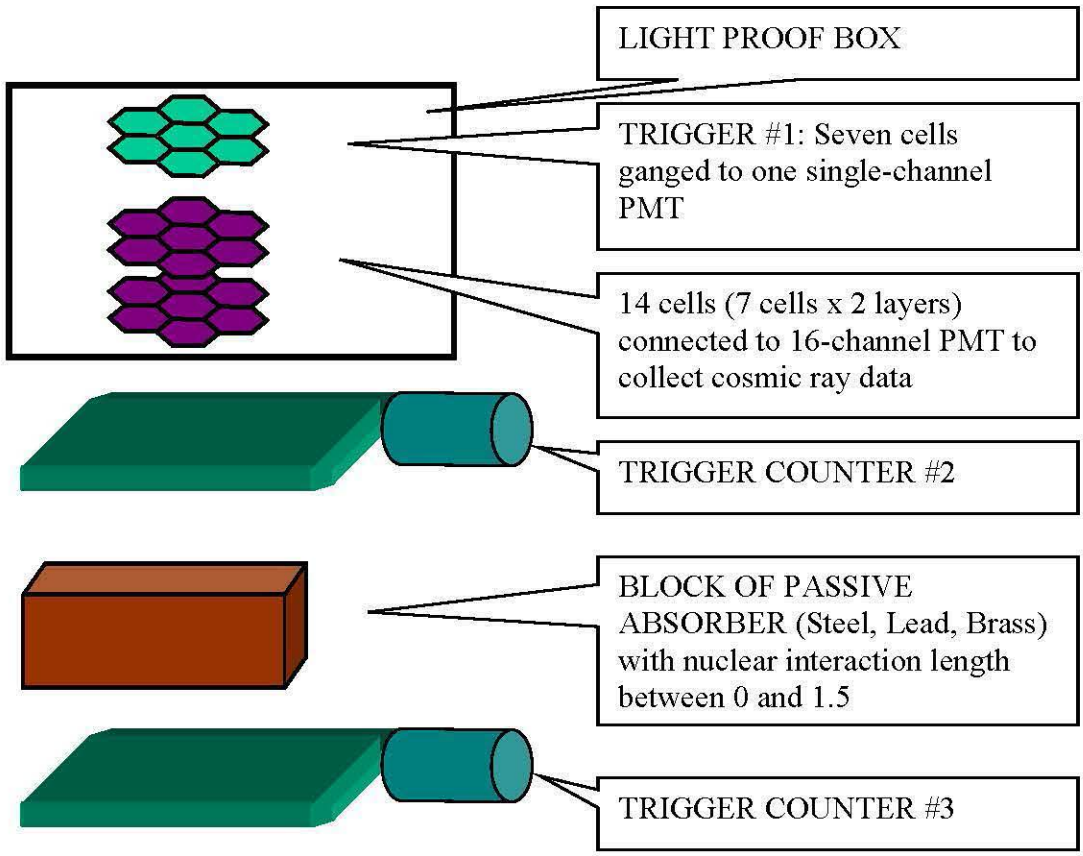

Fig. 3: Diagram of the cosmic ray test stand.

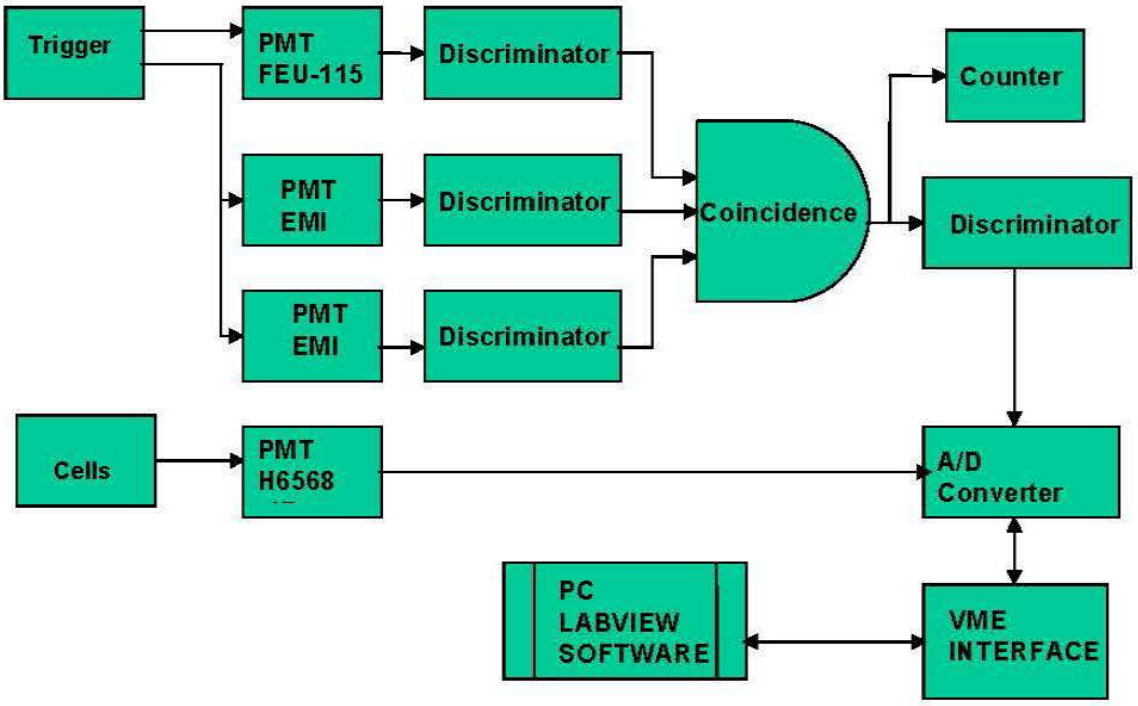

Fig. 4: Block diagram of triggering and data collection electronics.

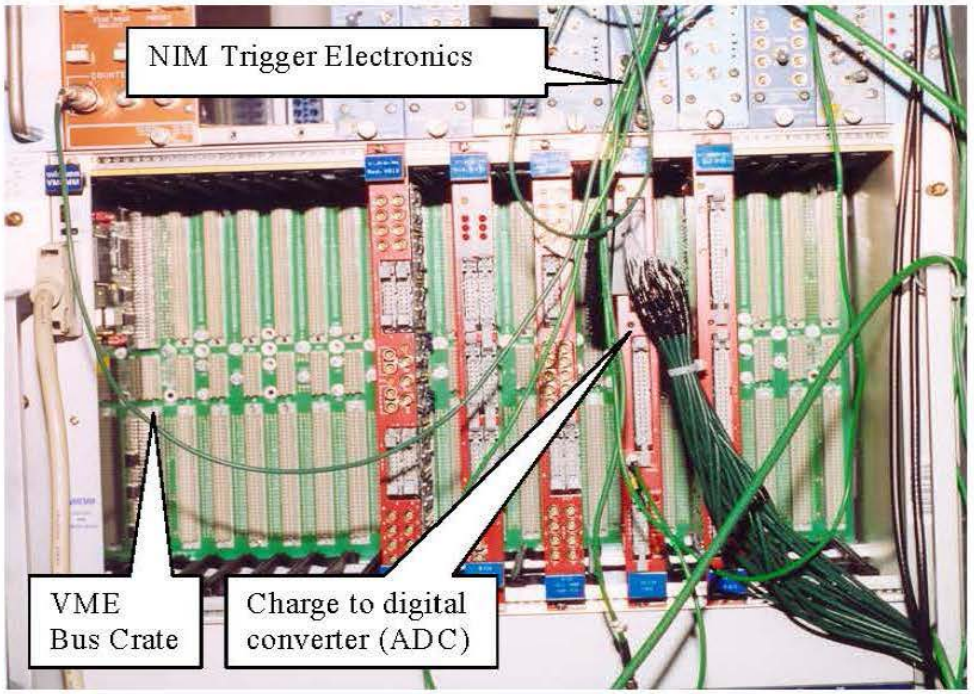

Fig 5: Picture of electronics hardware.

As shown in Fig.6, the analysis software is designed to display the data arranged by cell or by PMT channel. The cells were numbered based on the PMT channel to which they were initially connected. The histograms show the response of each cell in ADC counts for a series of triggered events.

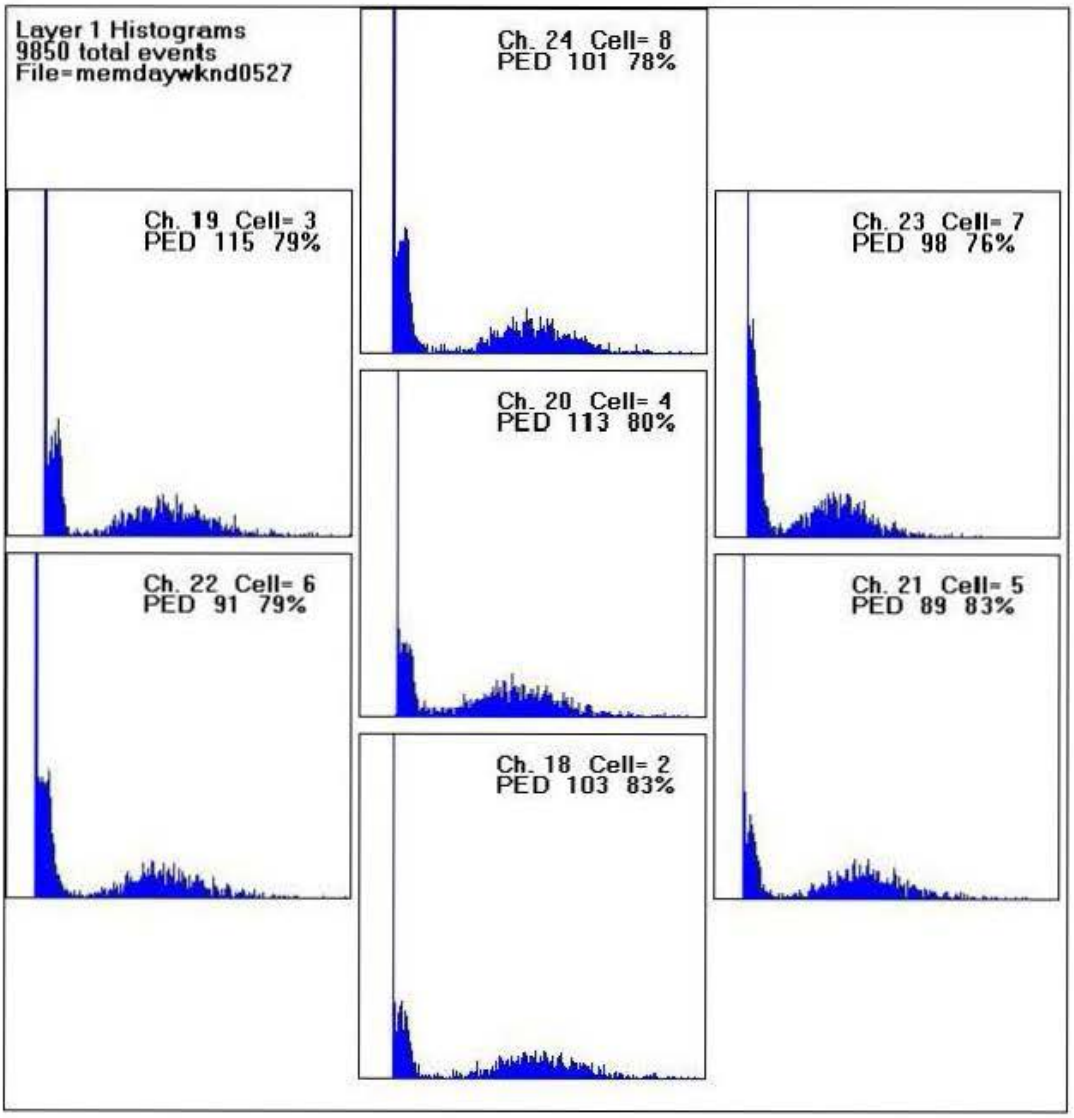

Fig. 6: Main window of the analysis software. The relative position of the cells is correct; the channel numbers are established by PMT convention.

The data can also be displayed in scatterplots. The scatterplots in Fig.7 show the response of each channel correlated with a single selected channel, in this case channel/cell #4. Cell #4 is located in the center of the top layer. As expected, cell #4 correlates perfectly with itself. The signals from the surrounding cells of the first layer appear to be uncorrelated. In the second layer, the outermost cells also are mostly uncorrelated. However, the center cell of the second layer, cell #9, which is directly below cell #4, is strongly correlated with cell #4.

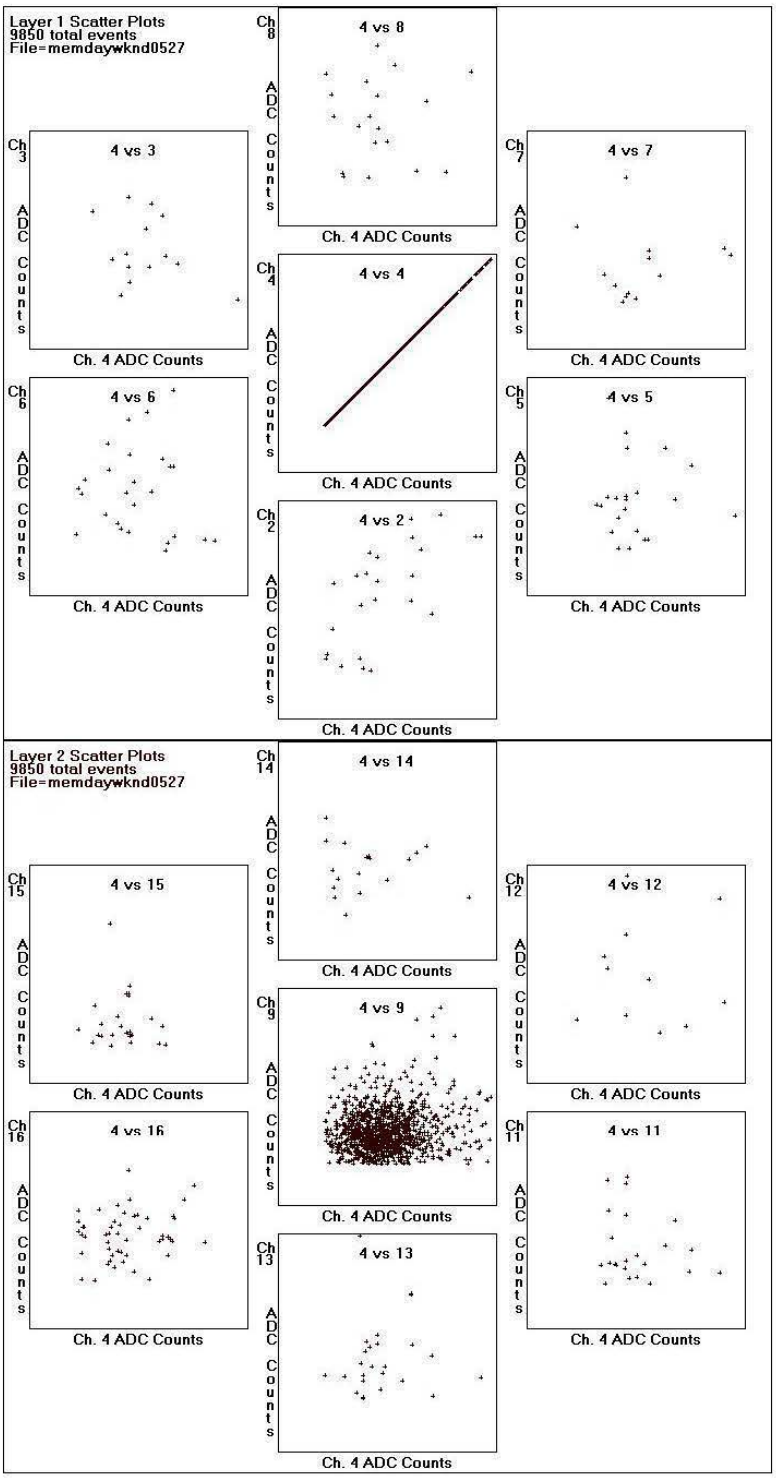

Fig. 7: Scatterplots showing the response of all cells relative to cell four. Only MIP events are shown.

CHAPTER 3

ANALYSIS OF DATA

3.1 Pedestal

Initial observations of the data for a single channel reveal the electronic pedestal and two peaks. The pedestal is due to events in which no particle passed through the cell. This is most likely to occur when a particle passed through the three triggering counters, causing the trigger signal, but passed through one of the other cells. The pedestal is nonzero because there is always some signal from the PMT. The pedestal range for the PMT and ADC system is 50 to 150 ADC counts, depending on the channel. The pedestal is the base level from which all other signals are referenced.

3.2 MIP Curve

As depicted in Fig. 8, the second curve to the right of the pedestal is the minimum ionizing particle (MIP) signal and has a Gaussian shape. Tests with a single-channel PMT were done with and without absorber material placed between Trigger 2 and Trigger 3. The absorber consisted of two pieces of 38mm thick steel, two 49mm thick lead bricks, and one 72mm thick brass cylinder. Lead has a nuclear interaction length (λ_{int}) of

170mm, the steel was treated as iron with a λ_{int} of 168mm, and the brass was treated as copper with λ_{int} = 151mm. A nuclear interaction length of ~1.5 was calculated for this configuration[5]. The mean of the Gaussian distributions with and without absorber were approximately the same, within 5 ADC counts. Since there was no significant change when the absorber was added, the absorber appears to be unnecessary for acquiring the MIP signal. Absorption in the building overburden is probably sufficient to acquire the MIP.

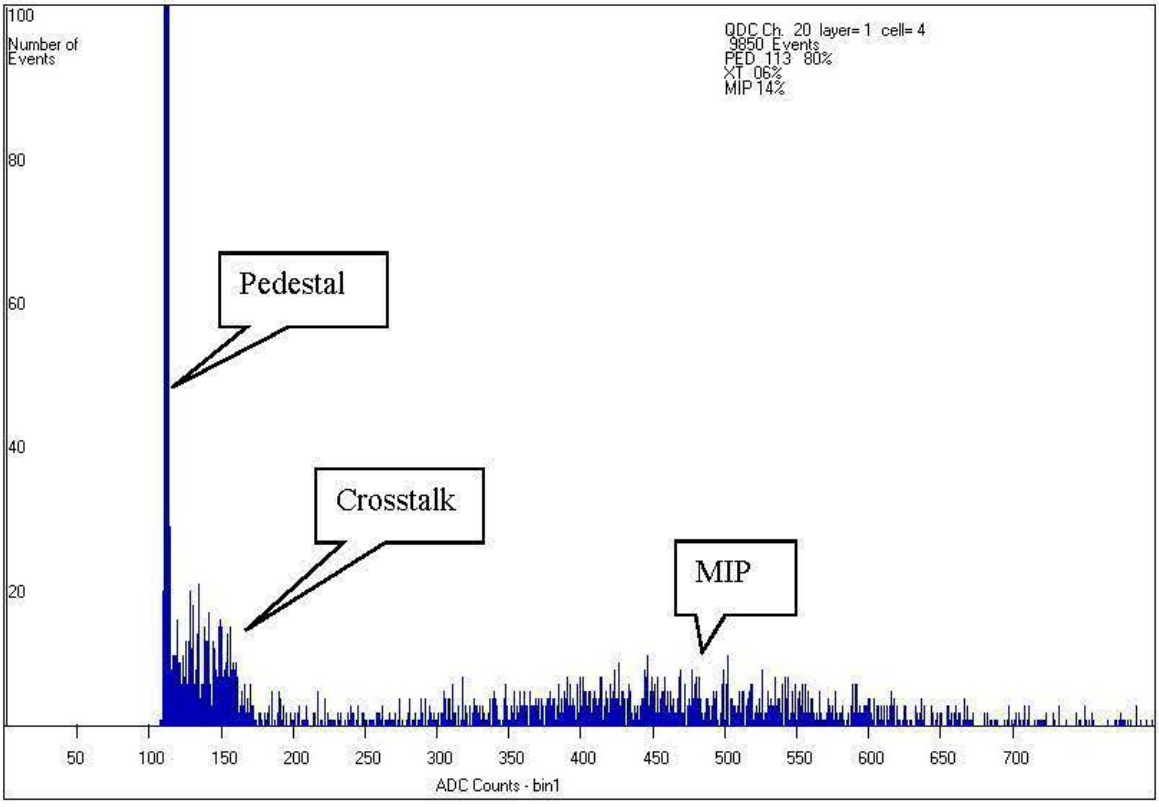

Fig. 8: Example histogram.

CHAPTER 4

ANALYZING CROSSTALK

4.1 Demonstration of Crosstalk

The first peak between the pedestal and MIP curve is due to crosstalk. Crosstalk is an additional component of the signal that is caused by an activity in another channel rather than the cell, fiber, and electronics of the first channel itself. This could be caused, for example, by some of the light generated by a cosmic ray leaking between cells. To exclude the possibility that this may be a MIP signal, channel four was isolated from all the other cells with black paper and all the other fibers were disconnected from the PMT channels. The resulting histogram, Fig. 9 shows a marked decrease in the first peak, indicating that the majority of the events in that range is crosstalk from the other channels.

4.2 Isolating the Cells

One source of crosstalk can be optical crosstalk between adjacent cells. Light generated in one cell by a cosmic ray can travel into an adjacent cell and generate a small signal there. The cells we used had been painted with white paint to create a stronger signal in a particular cell by reflecting light back into that cell.

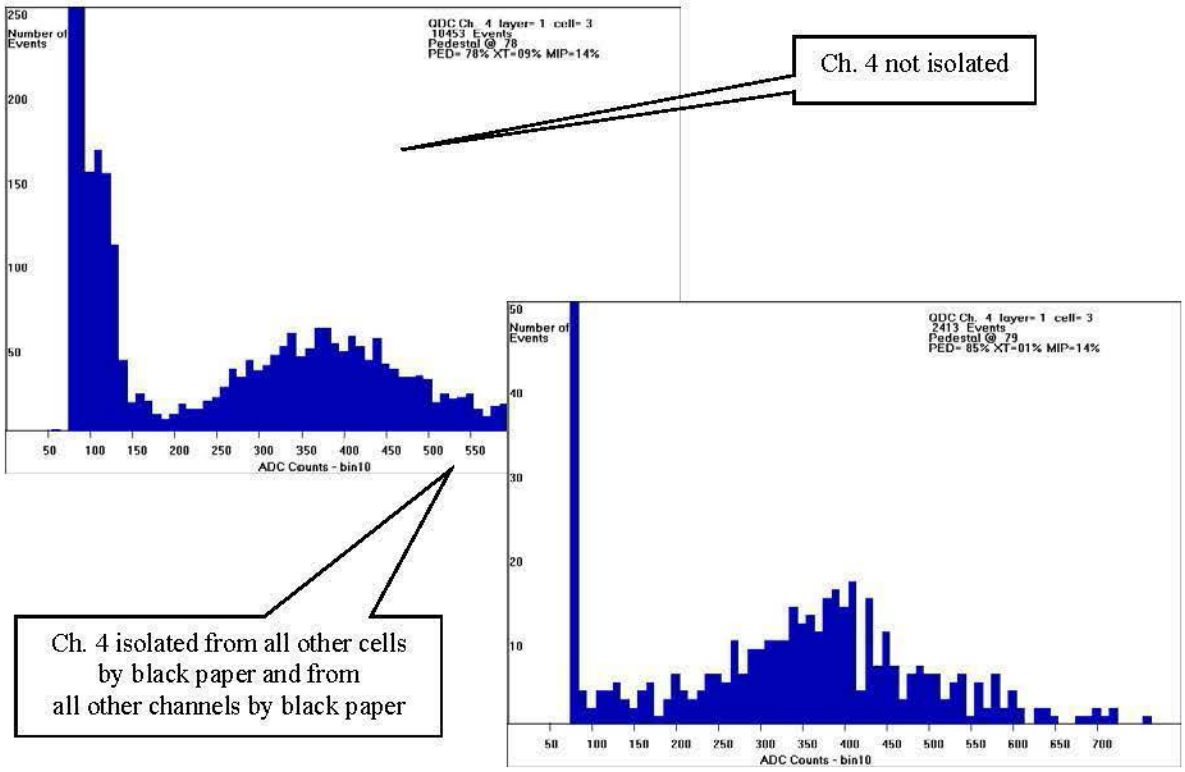

Fig 9: Before and after isolation of channel four.

Three of the cells were completely isolated and the two layers separated by black paper. Fig. 10 shows the percent of total events in the crosstalk range (i.e., not in pedestal and not part of the MIP curve) before and after isolating the cells. As can be seen, each cell demonstrates about 10-25% crosstalk reduction after increased isolation. Cell #5 has no change but this was later determined to be due to a weak input channel on the ADC and not on the PMT or cell. All other cells show a decrease in crosstalk events by 13 to 45%. All later data was collected with the cells isolated from other cells with black paper.

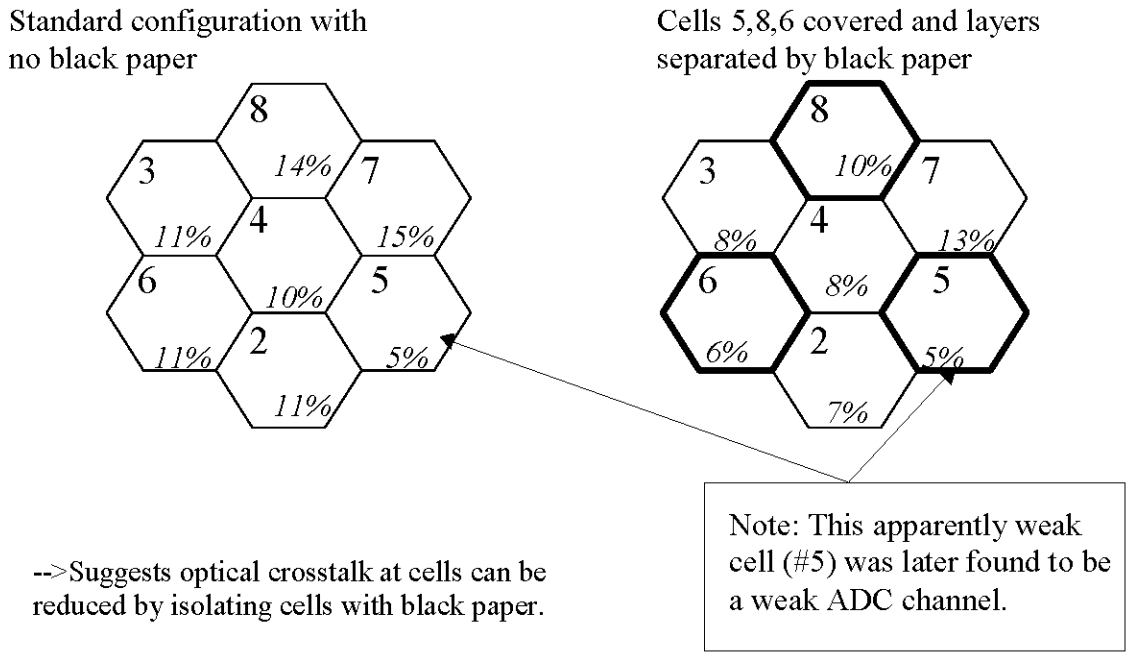

Fig. 10: Crosstalk before and after isolating cells 5, 6, and 8. The cell number is in the upper left of each cell. The percentage of the ADC distribution in the crosstalk region is given in italics.

4.3 Analyzing Crosstalk at the Photomultiplier Tube

To analyze crosstalk at the PMT only one cell (in this case #4) was connected for cosmic ray data. As can be seen from the scatterplots in Fig. 11, channel four correlates perfectly with itself as expected. However, there is still signal data indicated in the plots of the other adjacent channels. This "signal" must be crosstalk at the PMT from channel four. The relative strength of this crosstalk is shown in Fig. 12.

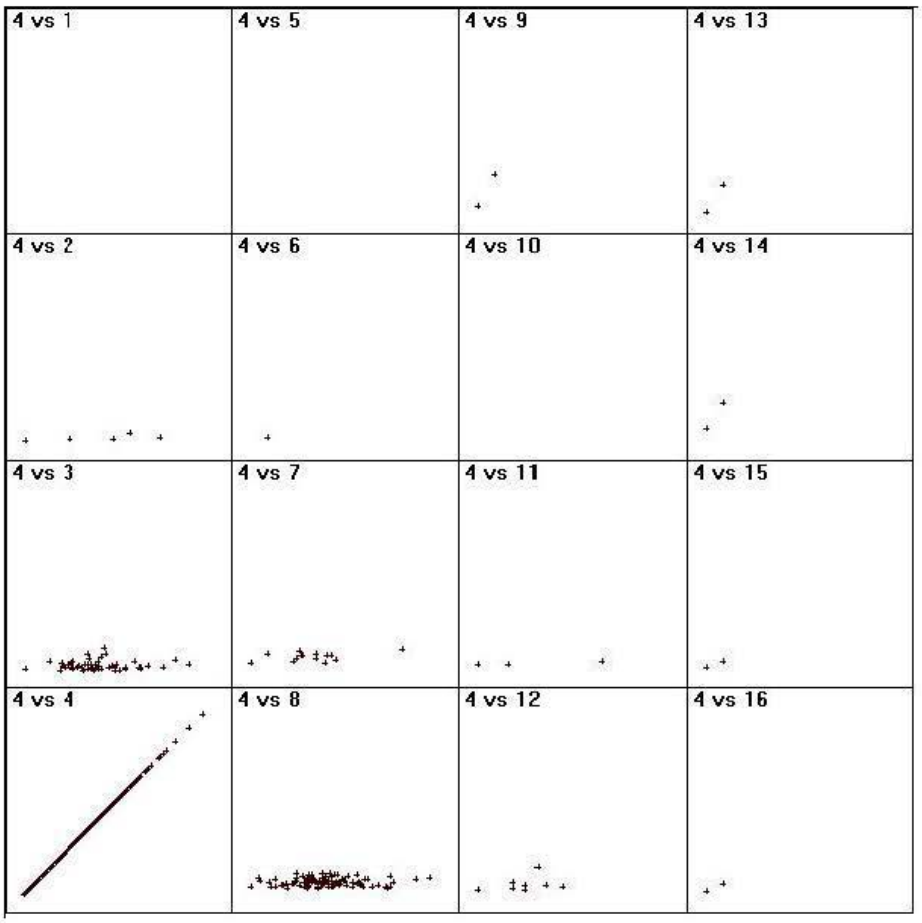

Fig. 11: Abbreviated scatterplot map arranged by PMT channel. The ADC counts of channel four are mapped versus all the other channels. Only MIP events are displayed. MIP events are those events with an ADC count greater than pedestal plus 50.

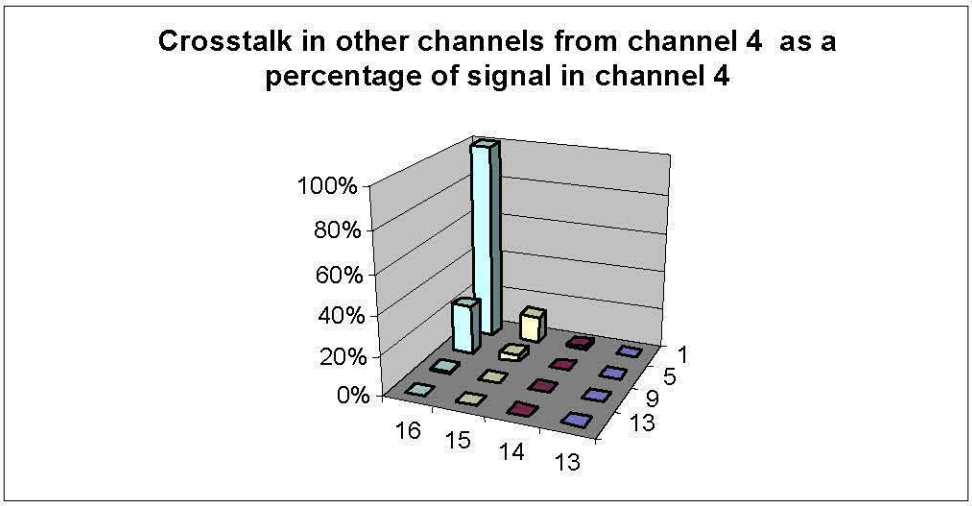

Fig. 12: Channel map of signal with only channel four connected.

At the PMT a channel can inject about 10-20% of its signal into other channels. PMT crosstalk is also a function of PMT high voltage. The voltage was set at 1000V for data runs. This voltage is somewhat higher than the 800V recommended by the PMT manufacturer[8]. One thousand volts was selected to increase the gain at the cost of increasing noise. This noise appears as the interchannel crosstalk.

4.4 Summary of Crosstalk Issues

A portion of the total crosstalk is optical crosstalk between cells. We can reduce optical crosstalk by covering cells with black paper. Another option would be to paint cells with black paint.

A greater part of the crosstalk occurs at the PMT. Some of this may be due to optical diffusion in the photocathode cover but is more likely caused by electrical

crosstalk between the dynodes of adjacent channels. This can be reduced by using a lower PMT voltage. This crosstalk is significant only on adjacent channels.

With the PMT HV set at 1000V and all the cells isolated with black paper, the crosstalk events are in the range of 5 to 13 % of the total events with the average being 8%. In comparison, 9 to 14% of the events are in the MIP range with the average being 12%.

In Fig. 13 efficiency is compared to noise rejection as a function of threshold. The efficiency is the percentage of signal or MIP events accepted for a particular threshold given as number of ADC counts. The noise rejection is the percentage of noise events, including pedestal and crosstalk, rejected for that particular number of ADC counts or lower. The signal and noise distributions were fit with two curves and the area under the two curves either side of the threshold was used to calculate the efficiency and rejection. For cell 4 the two curves cross at a threshold of 160 ADC counts or 47 ADC counts from the pedestal. At this point 99% of the noise has been rejected. All other channels show similar behavior, and 50 ADC counts from the pedestal were taken to be a reasonable cutoff between noise and signal. The digital hadron calorimeter thresholds will be determined by the crosstalk rather than the pedestal. Fig. 14 plots noise rejection percentage as a function of efficiency and indicates that 95% of the noise is rejected at an efficiency of 99%.

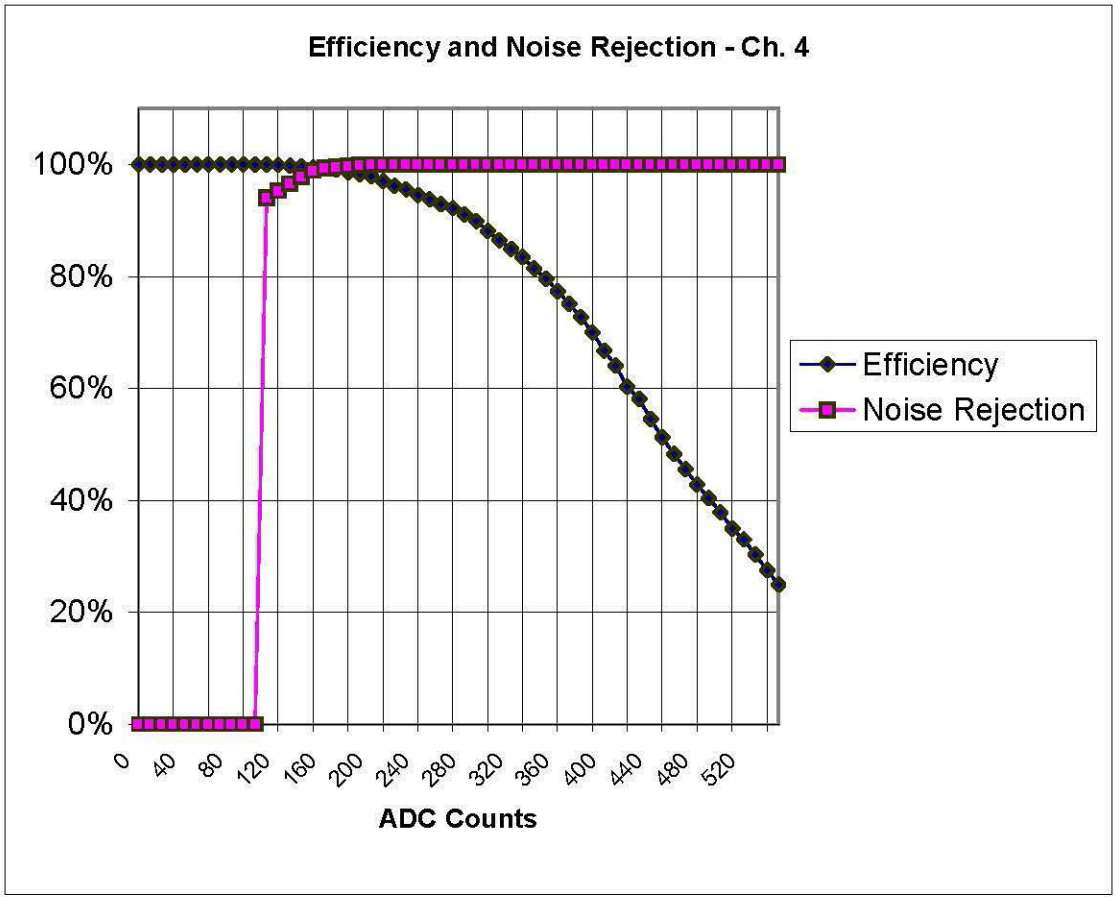

Fig. 13: Efficiency and noise rejection for channel four.

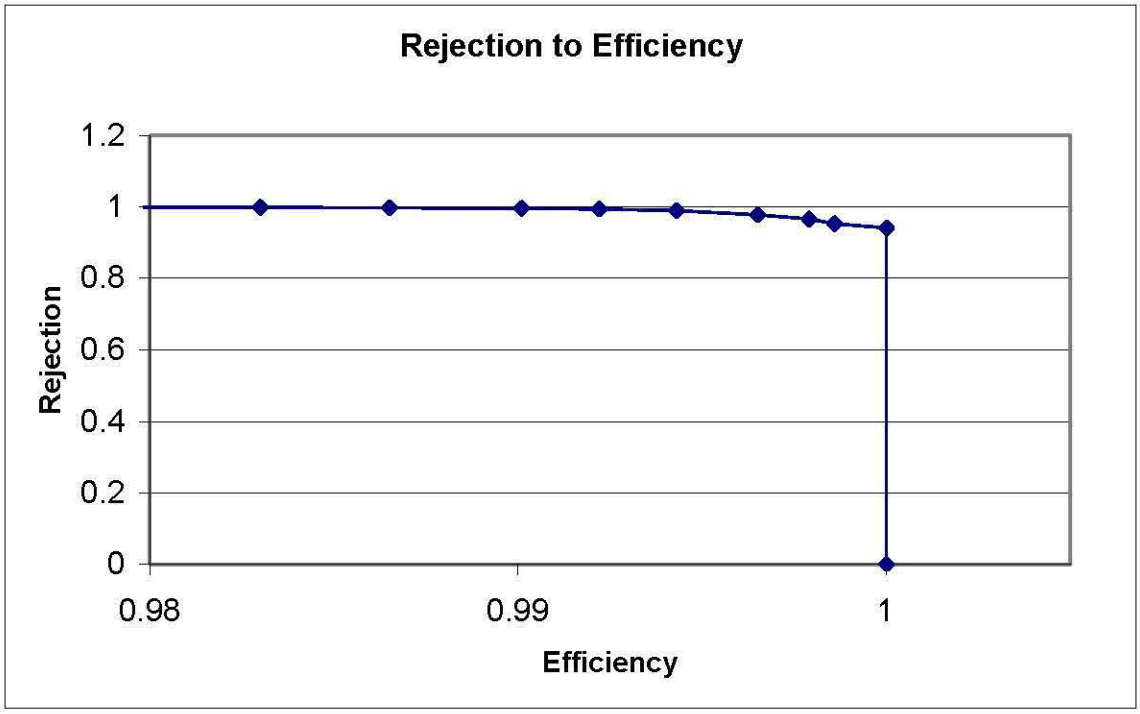

Fig. 14: Noise rejection percentage as a function of efficiency for channel four.

CHAPTER 5

CALIBRATION AND LIGHT YIELD

The light yield of the scintillating cells can be determined by taking the average from a cosmic ray distribution and dividing it by the average from a single photoelectron distribution. The first step then is to calibrate the system by measuring the number of ADC counts between the single photoelectron peak (SPE) and the pedestal.

A set of statistics from cosmic ray data will yield a Gaussian histogram with an average a certain distance from the pedestal. Every distribution far from the pedestal is really the sum of several distributions from integral numbers of electrons emitted by the photocathode, i.e. 1,2,3,4…n electrons. If the PMT photocathode is stimulated by a "large" amount of light, the higher number of electron channels will dominate and the composite distribution will be Gaussian with high amplitude and an average far from the pedestal. As the amount of light is lowered, the contribution to the total by the higher electron numbers is reduced. Both the average and the amplitude go down and a Landau distribution emerges[10].

At some low level of light, a pedestal will appear. As the level of light is further lowered, the average will approach the pedestal. The distribution will merge with the pedestal distribution, but there will still be a separation between the peaks. The total distribution will still be a sum of several electron distributions. However, the single photoelectron distribution will dominate in this case.

As the amount of light is further reduced, the average of the distribution will stay at the same distance from the pedestal because there cannot be fractional photoelectrons. However the amplitude will decrease and any contributions for higher photoelectron numbers will also decrease until there are only the single photoelectron and pedestal distributions. The difference between the single photoelectron peak and the pedestal in ADC counts is needed to determine the light yield. At some point when the light amplitude becomes so low the single photoelectron distribution will merge with the pedestal and become just a tail of the pedestal.

A calibration procedure is then suggested. Start with light amplitude high enough to generate a Gaussian distribution with no pedestal, then systematically reduce the light by increments. The average will decrease and the pedestal will grow in amplitude accordingly. When successive test runs show no change in the average, but instead an amplitude decrease, the single photoelectron distribution will be evident (V.Rykalin, personal communication, 2003).

Photographic filter material (neutral gel filters, Kodak No.96 N.D. 0.20 = 63% transmission) was used to attenuate light illuminating cell #4. Data was collected with 0 to 8 filter layers. A green LED was used to illuminate a single PMT photocathode (in this case channel four) through a clear optical fiber. The LED was driven at 16.7 Volts and 50Hz with a pulse of 22.3 ns. The LED drive signal was also used to generate the ADC trigger signal. As Fig. 15 demonstrates, as the amount of light is decreased by adding filter layers, the average of the histogram decreases and a pedestal appears and increases.

The average is the same in histograms Fig. 15 F and G, indicating that the peak of

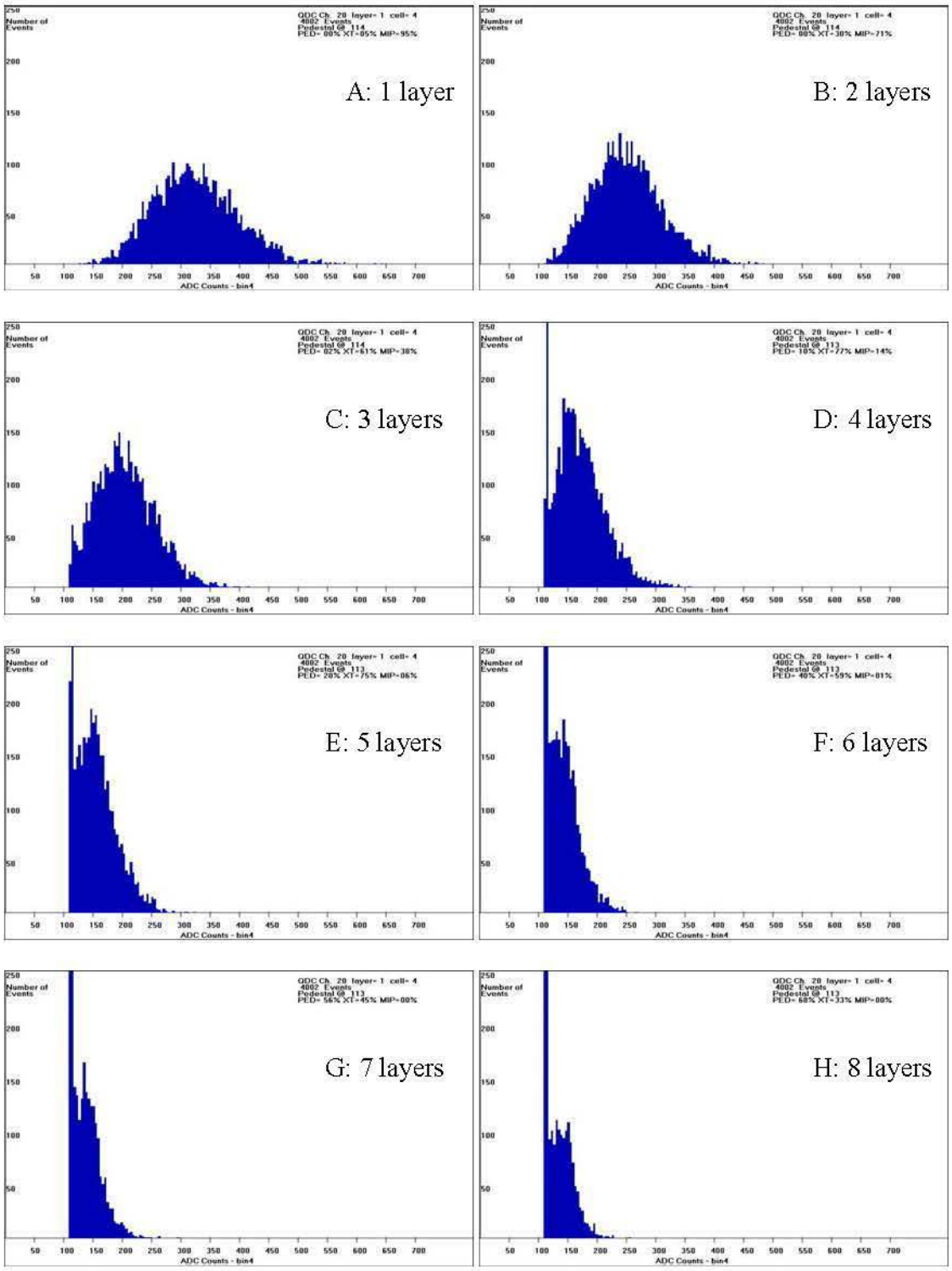

Fig. 15: Shifting of single photoelectron spectrum peak relative to pedestal as filter layers are added.

the of the single photoelectron spectrum has been found.

Fig. 16 graphs the histogram average of the nine data sets. For filter layers 6 through 8 the average does not change significantly. This corresponds to an ADC count of approximately 31 between the pedestal and channel four signal. Note also in Fig. 16 that after four filter layers the curve flattens. This point, about 50 ADC counts, can be used to set a digital threshold. Anything less than 50 ADC counts can be rejected as crosstalk and anything above 50 can be accepted as a MIP. This result complements what was already seen from studies of crosstalk discussed in Section 4.4.

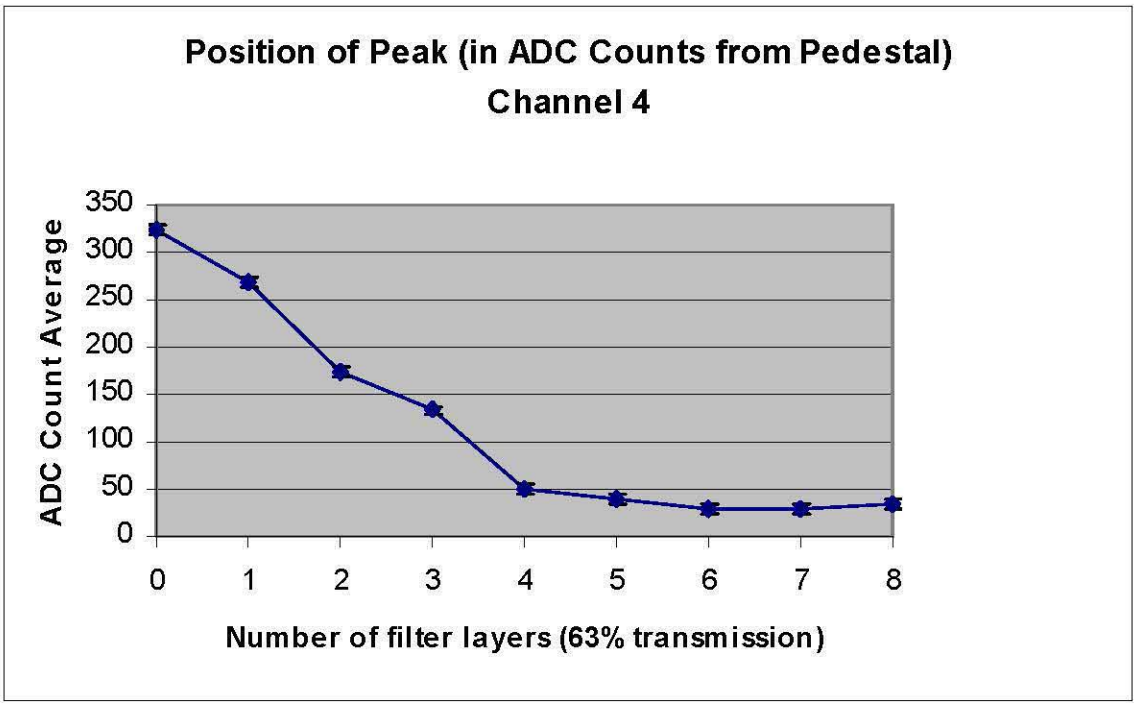

Fig. 16: Photoelectron peak as a function of layers of filter material.

The light yield is the average number of photoelectrons in the data distribution. It equals the average of the data distribution (in ADC counts) divided by the average of the single photoelectron peak (in ADC counts) referenced from the pedestal.
For channel four the pedestal=113 ADC counts, the single photoelectron peak is at 153 counts and the MIP peak is at 480 counts. The light yield would be L.Y. = (480-113)/(153-113) = 9.2 +/-1.4 P.E/M.I.P.

Table 1 column 7 shows the light yield for the cells. The calculation for cell #4 was performed in the method described above. The light yields from all the other cells were calculated using SPE peaks from data collection runs that used three layers of Tyvek material instead of the photo filter. Three layers of Tyvek were found to be equivalent to the five layers of photo filter in tests with channel four; therefore, the same material was used for all of the other channels. Since the photo filter is specifically designed to attenuate light and has clearly documented absorption properties, it is preferred to Tyvek.

The position of the pedestal in ADC counts is a function of the PMT, the PMT operating voltage, and individual variation in the PMT channels and the ADC. Since the pedestal is subtracted from both the MIP and single photoelectron (SPE) peaks, it is removed from the light yield calculation. The light yield is therefore not dependent on the PMT channel or ADC. The available data does not rule out other effects such as properties of the individual fibers. However, the strongest correlation is between the light yield and the individual cell. The range of light yields for the set of 14 operating cells is shown in Fig. 17. The mean = 9.8 and the variance =4.0.

Table 1. Light Yield and ADC Count Data

Cell Number / PMT Channel	Pedestal (raw ADC counts)	SPE (raw ADC counts)	MIP (raw ADC counts)	SPE (ADC counts less pedestal)	MIP (ADC counts less pedestal)	Light Yield (S.P.E./M.I.P. All use Tyvek filter except cell 4.)
2	103	138	540	35	437	12.5
3	115	153	480	38	365	9.6
4	113	153	480	31	367	9.2
5	89	123	460	34	371	10.9
6	91	121	480	30	389	13.0
7	98	125	380	27	282	10.4
8	101	136	520	35	419	12.0
9	86	118	340	32	254	7.9
11	97	130	320	33	223	6.8
12	105	137	400	32	295	9.2
13	79	114	380	35	301	8.6
14	72	103	340	31	268	8.6
15	69	101	280	32	211	6.6
16	111	141	420	30	309	10.3

Note: The data set was taken from 5/25/03 to 5/28/03. The data is arranged by PMT channel. Cell/Channel 1 and 10 were not connected.

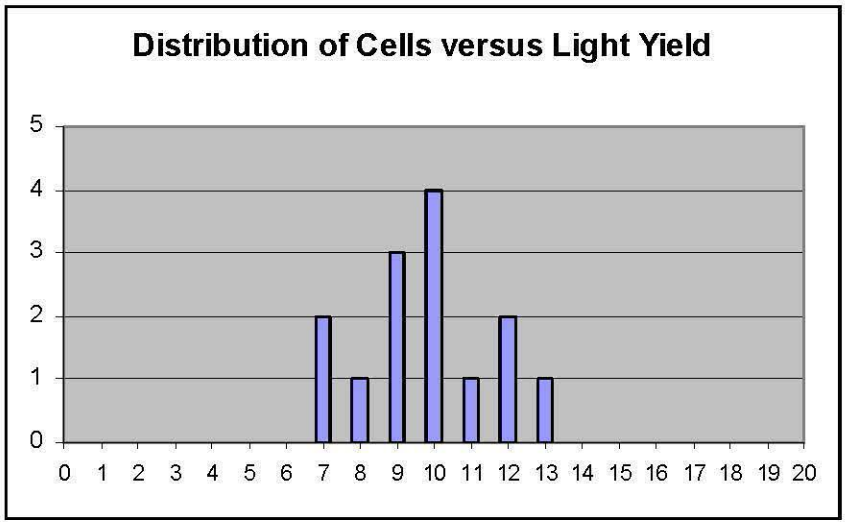

Fig. 17: Number of cells versus light yield.

CHAPTER 6

CONCLUSIONS

We have developed a cosmic ray test stand and a scintillating cell array to prepare for a digital hadron calorimeter. Crosstalk between cells can be up to 25% of the total signal. Optical crosstalk between cells represents 30% to 40% of the total crosstalk. Most of this is due to the cell immediately below the cell in question and can be reduced by isolating cells with black paper or paint. Crosstalk between adjacent channels at the PMT is 60 to 70 % of total crosstalk. Some component of this may be optical due to a finite thickness of the PMT photocathode window. Rejection versus efficiency studies show that single-channel thresholds can be set that efficiently reject noise while accepting MIP signals.

When developing a calorimeter using a large number of small cells, the cells should be uniform in terms of light yield. It is therefore important to develop a procedure to determine the single photoelectron spectrum peak and to use that data to calculate the light yield of the cells. The procedure we used to find the SPE used an LED driven by a pulse generator and layers of filter material. The SPE peak can also be used to establish a digital cutoff when switching from an analog to a digital calorimeter. The SPE and MIP averages can be used to determine cell light yields. The light yield has a range of 7 to 13 P.E./MIP. The cell light yields in our test set vary by a factor of 2.

The next step in DHC development is construction of a test stand with 12 layers of seven cells each separated by an absorber layer. The new test stand will allow us to track cosmic rays through the layers and to evaluate other techniques needed to realize digital hadron calorimetry on a larger scale.

REFERENCES

[1] Kondo, T. (2002). *Present Status of LHC and Prospects with Higher Luminosity* [On-line report]. Retrieved October 1, 2003: http://conference.kek.jp/RPIA2002/talks/kondo.pdf

[2] Maciel, A. (2002). *Simulation Studies for a Digital Hadron Calorimeter* [On-line report]. Retrieved October 1, 2003: http://www-sldnt.slac.stanford.edu/nld/meetings/2002/20020507/StMalo.pdf

[3] Oreglia, M. (2003). *Towards an International Linear Collider* [On-line report]. Retrieved October 1, 2003: http://hep.uchicago.edu/~oreglia/docs/fnal030606.pdf

[4] Chakraborty, D. (2002). *Calorimetry Summary* [On-line report]. Retrieved October 1, 2003: http://scipp.ucsc.edu/LC/talks/chakraborty_summary.ppt

[5] Wigmans, R. (2000). *Calorimetry: Energy Measurements in Particle Physics.* Oxford: Clarendon Press.

[6] Dyshkant, A. (2003). *Scintillating Digital Hadron Calorimeter Status and Plans for NICADD/NIU and UIC* [On-line report] Retrieved July 27, 2003: http://nicadd.niu.edu/meetings/dhcal/Dyshkant_CORNELL_2003_Scintillator_Digital_Hadron_Calorimeter_Status_And_Plan.ppt

[7] Bichsel, H., Groom, D.E., Klein, S.R. (2002). Passage of Particles Through Matter. *Physical Review D: Particles and Fields, 66*, 195-206

[8] Hamamatsu Photonics (2001). *Photomultiplier Tubes and Assemblies.* Toyooka-village, Iwata-gun, Shizuoka-ken, Japan: Hamamatsu Corporation.

[9] National Instruments (1996). *LabView User Manual.* Austin, Texas: National Instruments Corporation.

[10] Flyckt, S-O., Marmonier, C. (2002). *Photonis Imaging Sensors , Photomultiplier Tubes Principles and Applications.* Brive, France: Photonis.